# 3D-Modeling of thermal degradation of spruce wood under inert atmosphere

Hassan Flity, Mariam Abdo, Lucas Terrei, Zoubir Acem, Rabah Mehaddi, Paul Lardet, Gilles Parent

# 3D-Modeling of thermal degradation of spruce wood under inert atmosphere

Hassan Flity[a,b], Mariam Abdo[a,c], Lucas Terrei[a], Zoubir Acem[a], Rabah Mehaddi[a], Paul Lardet[b],Gilles Parent[a*]
[a]Université de Lorraine, CNRS, LEMTA, F-54000 Nancy, France.
[b]Université Paris-Est, CSTB, F-77447 Champs-sur-marne, France.
[c]Université de Lorraine, INRAE, LERMAB, ERBE, F-88000 Epinal, France.
*Corresponding author: gilles.parent@univ-lorraine.fr

## Highlights:

- Thermogravimetric analysis of wood.
- Experiments at the cone calorimeter using thermally inert material.
- 3D-Modeling of wood thermal degradation at the cone calorimeter scale.

## Abstract:

The aim of this work was to model the thermal degradation of wood in an inert atmosphere at the cone calorimeter scale. First, the degradation of spruce wood was studied at the matter scale by TGA and DSC in an inert atmosphere at different heating rates. The kinetic parameters associated with a global multi-reaction mechanism were estimated by fitting the mass loss and the mass loss rate obtained by the TGA. The heats of reaction associated with the reaction scheme were estimated by fitting the heat flux measured by DSC. Then, experiments with an inert material (calcium silicate) were performed at the cone calorimeter scale under an inert atmosphere to characterize the boundary conditions of the developed 3D heat transfer model. The boundary conditions were determined by minimizing the difference between the measured in-depth temperatures and the predictions of the model using a least squares method. The results showed good predictions in agreement with experimental data and the convective heat transfer coefficients obtained were realistic. Finally, a 3D pyrolysis model, taking into account the anisotropic nature of wood, was developed by coupling the heat transfer with the kinetic model. The latter model was validated by comparison with tests carried out on spruce wood in an inert atmosphere using a cone heater.

**Keywords:** Wood; Thermal degradation; 3D-Pyrolysis model; Thermogravimetric analysis; Cone calorimeter

## 1. Introduction

Wood is a material with interesting thermal and mechanical properties and its carbon footprint is one of the lowest among building materials [1, 2]. Unfortunately, the fire behavior of wood limits its use in buildings [3]. A better understanding and control of the fundamental processes of wood combustion, in particular the primary pyrolysis phase, can help to reduce the constraints on the use of wood as a building material.
This topic is mainly studied at matter scale using TGA [4, 5, 6] under inert atmosphere. At this scale, the sample mass is very small (4 to 50 mg) and the sample is thermally thin, so heat transfer can be neglected and a 0D model can be used to predict the mass loss. Several mechanisms have been proposed in the literature to predict the mass loss and the mass loss rate obtained from TGA. These mechanisms can be divided into two

main categories. Some studies consider the wood as a homogeneous material for which thermal degradation occurs according to a single step [7], consecutive steps [8], parallel reactions [9] or a combination of parallel and consecutive reactions [10]. Other authors consider that this description is not sufficient to predict the thermal degradation of wood, which should rather be considered as the sum of the degradation of its main components: hemicellulose, cellulose, lignin [11, 12]. Models of these two categories have advantages and drawbacks: more or less complex, more or less predictive. However, the results of all of them are satisfactory in 0D.

In the context of building fires, wood materials are thermally thick, requiring the study of pyrolysis at larger scales. Today, the cone calorimeter is the largest scale at which the thermal degradation is studied in an inert atmosphere [8, 13]. At this scale, heat transfer controls the pyrolysis phenomena and must be taken into account. The multi-scale approach is used to model the degradation at this scale *i.e.* the kinetic parameters are estimated at 0D and used in a 1D or 3D model coupled with heat transfer. Several tools can be used to model the thermal degradation of materials *e.g.* Fire Dynamic Simulator (FDS), GPYRO [14], THERMAKIN [15]. Bustamante [16] showed the inadequacy of FDS to simulate cone calorimeter tests with kinetic parameters calculated from TGA. THERMAKIN cannot simulate 3D problems. Meanwhile, several studies have shown the ability of GPYRO to simulate materials degradation at a large scale. However, in GPYRO, thermal properties vary according to power laws and material properties are calculated according to mixture laws. The latter assumption is true for some properties such as the heat capacity, but it is not appropriate for the thermal conductivity. These features are two significant weaknesses of GPYRO. It is worth mentioning the studies conducted by Richter and Rein [17], as well as the study by Lautenberger and Fernandez-Pello [18], who utilized the GPYRO model to simulate the pyrolysis and oxidation of wood under three different oxygen concentrations: 0 %, 10.5 %, and 21 %. The models were validated on the basis of the experimental results obtained by Kashiwagi *et. al* [13] on samples of white pine, considering constant thermal properties. The results were quite good and the remaining discrepancies were attributed to the uncertainty in the boundary conditions, the material properties and their variation with temperature (in particular the thermal diffusivity of wood and char) and the kinetic parameters of char oxidation. It should be noted that Kashiwagi *et al*'s experiments [13] were performed on 3.8 cm side cubic samples, so the heat transfer can hardly be considered 1D in this case, especially for the in-depth temperature at locations far from the surface of the sample (temperature was measured up to 15 mm deep).

The aim of this study was to simulate the thermal degradation of spruce wood at the cone calorimeter scale in an inert atmosphere, following the work of Terrei *et al.* [8], but now using measured wood thermal properties and an improved modeling including in particular a 3D heat transfer (instead of 1D). First, wood was characterized at the matter scale thanks to TGA tests as it is commonly done. These tests were carried out at different heating rates. The kinetic parameters involved in a global multi-reaction mechanism were estimated by fitting the mass loss and the mass loss rate obtained by the TGA. More originally, DSC measurements were performed to determine the heats of reaction corresponding to the different reactions taking place in the material during its degradation. In a second step, tests were carried out at the material scale in inert atmosphere using the cone calorimeter. At this scale, particular attention was paid to the determination of the thermal boundary conditions. For this purpose, tests with an inert material were carried out with the same experimental conditions as the wood tests. An

inverse method using a 3D heat transfer model was applied to these tests to determine the boundary conditions. Finally, a 3D pyrolysis model was developed in PYTHON to simulate wood degradation at the cone scale. The model accounts for the anisotropic nature of wood. The kinetic parameters obtained from TGA and the boundary conditions obtained from the inert material tests were used in the 3D pyrolysis model. In addition, all properties of the model were measured experimentally except the thermal conductivity above 200 °C. The latter property was varied until the best agreement between numerical and experimental results was obtained. Since the model used is complex and most of its parameters have been measured experimentally, the thermal conductivity obtained should be reliable.

## 2. Matter scale

The aim of this section is to present the thermal degradation of spruce wood at the matter scale. For this purpose, the degradation of spruce wood in an inert atmosphere has been studied by TGA and DSC. At this scale, the spatial temperature gradients within the wood sample are negligible, thus only the kinetics of the chemical reactions occurring during pyrolysis is involved.

### 2.1 Thermogravimetric analysis

Dry solid wood samples with an initial mass varying between 4.5 and 5 mg were subjected to a temperature ramp from room temperature to 1000 °C at different heating rates of 5, 10 and 20 °C $\cdot$ min$^{-1}$. The tests were carried out under inert atmosphere using nitrogen with a flow rate of 80 mL$\cdot$min$^{-1}$ to avoid oxidation of the char and thus concentrate on the sole pyrolysis. The evolution of the sample mass as a function of the sample temperature, was continuously recorded. Fig. 1 shows the mean normalized mass loss and the mean normalized mass loss rate as a function of temperature for the different heating rates. For each heating rate, three repeatability tests were performed with a relative difference of approximately 1.3 %.

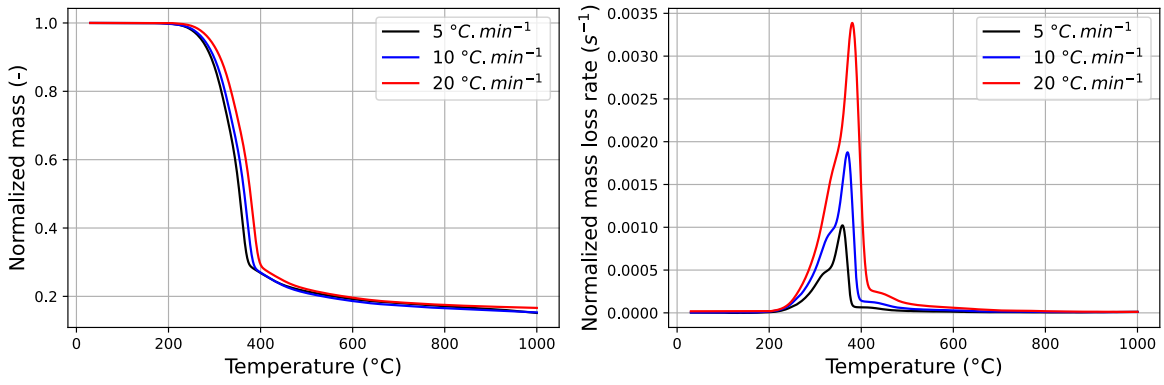


(a) Normalized mass loss (b) Normalized mass loss rate

Fig. 1. Mean normalized mass loss and mean normalized mass loss rate as a function of temperature for the different heating rates: 5, 10 and 20 °C $\cdot$ min$^{-1}$.

For a given heating rate, the observed stages of decomposition of the spruce wood are as follows:

- **Below 210 °C:** the mass of the samples remains constant.

- **At 210 °C:** the degradation of spruce begins and the mass of spruce starts to decrease.

- **Between 300 °C and 350 °C:** there is a peak in the mass loss rate. This peak corresponds mainly to the degradation of hemicellulose as reported in several studies [6, 8, 11].

- **Between 350 °C and 420 °C:** the main step of degradation occurs and a significant peak in mass loss rate is observed. During this stage, the wood looses more than 70 % of its initial mass. This step corresponds mainly to the degradation of cellulose [6, 8, 11].

- **After 420 °C:** the mass loss rate decreases slightly until a plateau is reached. This is due to the degradation of a part of the lignin. In fact, lignin degradation occurs over a wide temperature range, from 200 °C to 900 °C [19, 20].

Overall, the experimental results show that wood degradation follows the same trend regardless of the heating rate. However, Fig. 1 (b) shows a strong influence of the heating rate on the intensities of the mass loss rate peaks. Thus, the higher the heating rate, the higher the maximum mass loss rate. Fig. 1 (b) also shows that as the heating rate increases, the different mass loss rate peaks occur at higher temperatures. This behavior has also been observed in several studies [10, 11]. Indeed, when the heating rate is low, the temperature within the sample increases uniformly. On the other hand, when the heating rate is high, the temperature within the sample is no longer uniform and the temperature in the core of the wood is not exactly that of the reactor [12].

## 2.2 Kinetic model

Based on the experimental results, the model used to predict the wood degradation is a global multi-reaction model. In this model, dry wood is considered to be composed of three pseudo-solids $A_1$, $A_2$ and $A_3$, with initial mass fractions equal to $\alpha_1$, $\alpha_2$ and $\alpha_3$ respectively. These pseudo-components degrade simultaneously and independently according to first-order kinetic laws. $A_1$ degradation only leads to a gaseous constituent $G_1$, the decomposition of $A_2$ leads to a gaseous constituent $G_2$ and a char constituent $C_2$. The decomposition of $A_3$ leads to a gaseous constituent $G_3$ and a char constituent $C_3$. Further details of this model and the theory behind it will be published in a future paper which is currently under review. The reaction scheme adopted is therefore as follows:

$$A_1 \xrightarrow{k_1} G_1(\text{Gaz})$$

$$A_2 \xrightarrow{k_2} G_2(\text{Gaz}) + \gamma_2.C_2(\text{Solid})$$

$$A_3 \xrightarrow{k_3} G_3(\text{Gaz}) + \gamma_3.C_3(\text{Solid})$$

Where: $\gamma_2$ and $\gamma_3$ are the stoichiometric coefficients. $K_1$, $K_2$ and $K_3$ are the rate coefficients of the reactions which follow an Arrhenius law ($K_i$=$K_{0i}$.exp(-$E_i$/RT)). $K_{0i}$ and $E_i$ are the pre-exponential factor and the activation energy of the reaction i, respectively, T

is the temperature and R is the ideal gas constant. The mass balance of $A_1$, $A_2$, $A_3$, $C_2$ and $C_3$ are respectively:

$$\frac{dm_{A_1}}{dt} = -K_1.m_{A_1} \quad (1)$$

$$\frac{dm_{A_2}}{dt} = -K_2.m_{A_2} \quad (2)$$

$$\frac{dm_{A_3}}{dt} = -K_3.m_{A_3} \quad (3)$$

$$\frac{dm_{C_2}}{dt} = \gamma_2.K_2.m_{A_2} \quad (4)$$

$$\frac{dm_{C_3}}{dt} = \gamma_3.K_3.m_{A_3} \quad (5)$$

Where $m_{A_1}$, $m_{A_2}$, $m_{A_3}$, $m_{C_2}$ and $m_{C_3}$ are respectively the mass of the components $A_1$, $A_2$, $A_3$, $C_2$ and $C_3$. Eqs. 1, 2, 3, 4 and 5 were solved numerically to determine the mass of each component at the time t. Then, the total mass of the sample M(t) is calculated by:

$$M(t) = m_{A_1}(t) + m_{A_2}(t) + m_{A_3}(t) + m_{C_2}(t) + m_{C_3}(t) \quad (6)$$

The kinetic parameters of the model *i.e.* pre-exponential factors ($K_{01}$, $K_{02}$ and $K_{03}$), activation energies ($E_1$, $E_2$ and $E_3$) and stoichiometric coefficients ($\alpha_1$, $\alpha_2$, $\alpha_3$, $\gamma_2$ and $\gamma_3$) were estimated by simultaneously fitting the mass loss and the mass loss rate curves obtained by TGA. Levenberg-Marquardt algorithm [21] was used to minimize the following objective function:

$$S = \sum_{i=1}^{N} \left[M_{exp}(t_i) - M_{mod}(t_i)\right]^2 + \delta \sum_{i=1}^{N} \left[\frac{dM_{exp}}{dt}(t_i) - \frac{dM_{mod}}{dt}(t_i)\right]^2 \quad (7)$$

Where: N is the number of experimental points; $M_{exp}(t_i)$ and $\frac{dM_{exp}}{dt}(t_i)$ are the measured mass and mass loss rate, respectively; $M_{mod}(t_i)$ and $\frac{dM_{mod}}{dt}(t_i)$ are the corresponding numerical quantities. As the magnitude of the mass loss is extremely higher than the mass loss rate, the sum of the mass loss rate is multiplied by a factor ($\delta$) to increase the weight of the mass loss rate in the optimization. Several constraints were applied on the parameters during the optimization. Firstly, as there is a compensation effect between the pre-exponential factor and the activation energy [22], the algorithm could converge toward different sets of parameters. Thus, the activation energy was constrained to vary between 60 and 200 $kJ \cdot mol^{-1}$ which is the order of magnitude of this parameter in the literature. Table 1 shows the values of the kinetic parameters obtained by optimization. Fig. 2 shows that the model generally well predicts the normalized mass loss and the normalized mass loss rate obtained by TGA. A slight discrepancy is observed above 400 °C. This can be attributed to a delayed degradation of the third component $A_3$. In addition, this kinetic mechanism, with only three first order reactions, can be considered too simple to account for all the reactions that occur at high temperature.

### 2.3 Differential scanning calorimetry

The differential scanning calorimeter used in this study is the SETARAM DSC 111. This instrument has been modified and equipped with an original fixed-bed setup to ensure better control of sample scanning. Prior to performing the tests, the instrument

Table 1. The kinetic parameters obtained by optimisation.

| Reaction | $K_{0i}$ ($s^{-1}$) | $E_i$ ($kJ \cdot mol^{-1}$) | $\alpha_i$ (-) | $\gamma_i$ (-) |
|---|---|---|---|---|
| (1) | $7.1 \times 10^8$ | 123 | 0.17 | - |
| (2) | $1.3 \times 10^{12}$ | 173 | 0.61 | 0.1 |
| (3) | 552 | 81 | 0.22 | 0.59 |

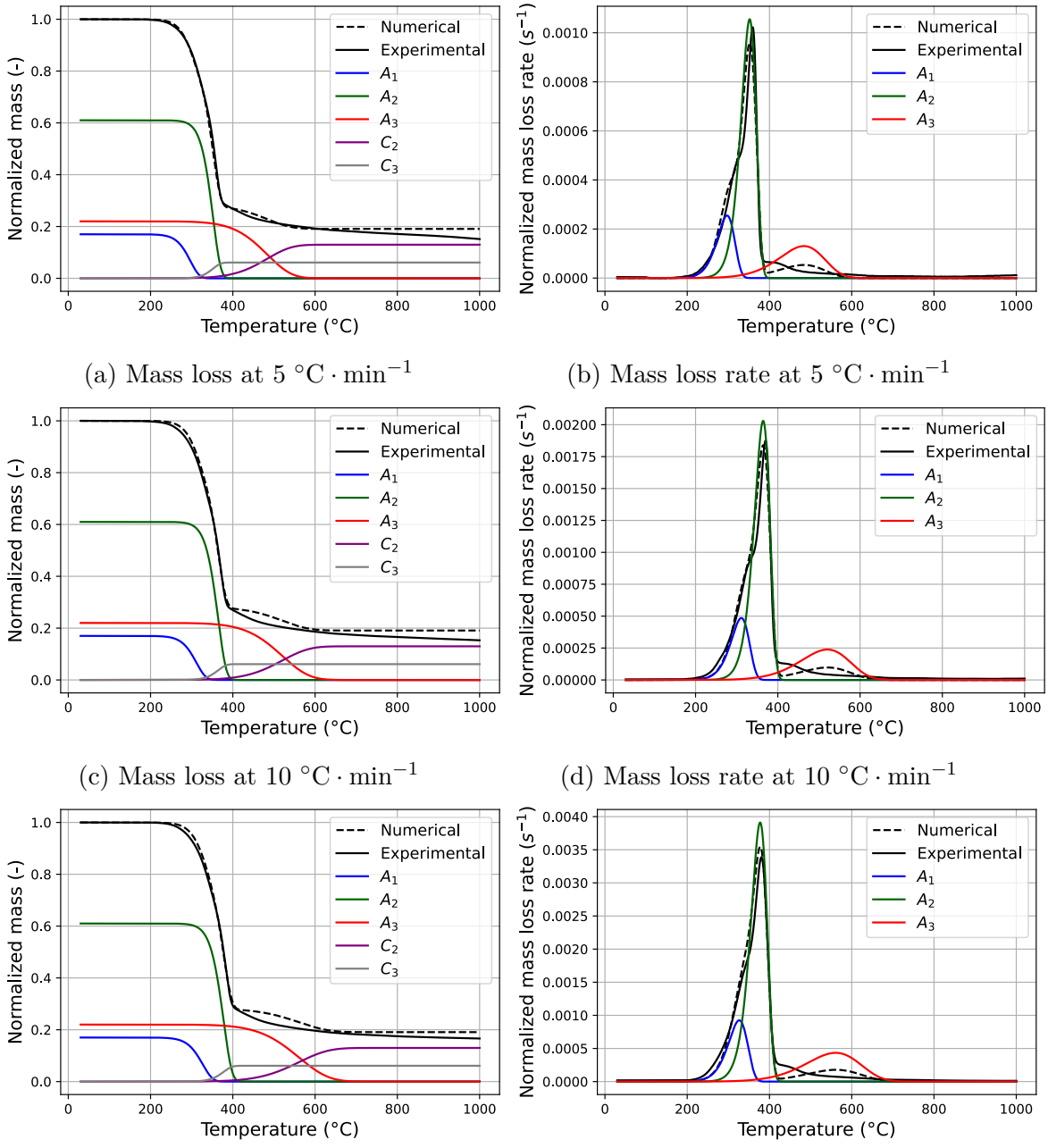


(a) Mass loss at 5 °C · $min^{-1}$

(b) Mass loss rate at 5 °C · $min^{-1}$

(c) Mass loss at 10 °C · $min^{-1}$

(d) Mass loss rate at 10 °C · $min^{-1}$

(e) Mass loss at 20 °C · $min^{-1}$

(f) Mass loss rate at 20 °C · $min^{-1}$

Fig. 2. Comparison between the numerical and experimental results for different heating rates. $A_1$, $A_2$, and $A_3$ are the pseudo-components of wood, while $C_2$ and $C_3$ are two char constituents.

was calibrated (temperature and sensitivity) using the melting temperature and enthalpy

of the following standard materials: indium, tin, lead and zinc. The calibration was performed under the same experimental conditions as the wood tests, i.e., the same heating rate, argon flow rate, and temperature program. Prior to each wood test, an empty tube test was performed to establish the baseline of the apparatus. The tests were performed at a heating rate of 10 $\mathrm{K} \cdot \mathrm{min}^{-1}$, ranging from room temperature to 600 °C, under an inert atmosphere using nitrogen at a flow rate of 20 $\mathrm{mL} \cdot \mathrm{min}^{-1}$. The samples tested were cylindrical with a diameter of 3.4 mm and a height of 6.5 mm. These samples were oven dried at 105°C for 24 hours prior to testing. Note that $Q_{total}^{exp}$ is the heat flux measured by the DSC, corrected by the instrument baseline and normalized by the initial mass of the sample and the heating rate. $Q_{total}^{exp}$ was assumed to be the sum of an effective heat capacity (sensible heat flux $Q_s$) and the heat of reaction $Q_r$. The effective heat capacity is assumed to be as follows [23]:

$$C_p(T) = (1 - X(T)).C_{p,wood}(T) \ + \ X(T).C_{p,char}(T).(\gamma_2 + \gamma_3) \tag{8}$$

Where: $(\gamma_2 + \gamma_3)$ is the final char yield, $C_{p,wood}(T)$ is the heat capacity of wood, $C_{p,char}(T)$ is the heat capacity of char and X(T) is the mass conversion defined by:

$$X(T) = \frac{m_0 - m(T)}{m_0 - (\gamma_2 + \gamma_3)} \tag{9}$$

Where $m_0$ and $m(T)$ are the initial mass and the mass of the sample at the temperature T calculated from the kinetic model, respectively. Therefore, the normalized heat flux measured by DSC can be modeled as:

$$Q_{total}^{num}(T) = \overbrace{(1 - X(T))C_{p,wood}(T) + X(T)C_{p,char}(T)(\gamma_2 + \gamma_3)}^{\text{Effective heat capacity } (C_p(T))} + \overbrace{\frac{1}{\beta}\left(\sum_{i=1}^{3} \frac{\frac{dm_{A_i}}{dt}(T)H_i}{\alpha_i}\right)}^{\text{Heat of reactions } (Q_r)} \tag{10}$$

Where: $H_i$ is the heat of reaction $i$, and $\beta$ is the heating rate. Finally, the heats of reactions $H_1$, $H_2$, and $H_3$ were estimated by minimizing the sum of the quadratic error between $Q_{total}^{num}$ and $Q_{total}^{exp}$. Fig. 3 (a) shows that the three reactions used to predict the mass loss at the macro scale were unable to predict the heat flux measured by DSC. Therefore, a fourth reaction was added, and the reaction scheme became as follows:

$$\mathrm{A_1} \xrightarrow{\mathrm{k_1}} \mathrm{G_1(Gaz)} \ + \ \mathrm{H_1}$$

$$\mathrm{A_2} \xrightarrow{\mathrm{k_2}} \mathrm{G_2(Gaz)} + \gamma_2.\mathrm{C_2(Solid)} \ + \ \mathrm{H_2}$$

$$\mathrm{A_3} \xrightarrow{\mathrm{k_3}} \mathrm{G_3(Gaz)} + \gamma_3.\mathrm{C_3(Solid)} \ + \ \mathrm{H_3}$$

$$\mathrm{C_2(Solid)} \xrightarrow{\mathrm{k_4}} \mathrm{C_4(Solid)} \ + \ \mathrm{H_4}$$

Where $H_1$, $H_2$, $H_3$, and $H_4$ are the respective heats of reaction 1, 2, 3, and 4. Note that in the fourth reaction, there is only heat production and no mass loss. In this reaction, the char $C_2$ is converted into another char $C_4$ with the same mass but a different morphology. In this case, the heat of reactions $Q_r$ in Eq. 10 becomes:

$$Q_r = \frac{1}{\beta}\left(\sum_{i=1}^{3} \frac{\frac{dm_{A_i}}{dt}H_i}{\alpha_i} + \frac{\frac{dm_{C_2}}{dt}H_4}{\alpha_2\gamma_2}\right) \tag{11}$$

Fig. 3 (b) shows that the kinetic scheme with 4 reactions predicts the experimental data very well. The following heats of reaction were obtained: $H_1 = -37.5\text{kJ} \cdot \text{kg}^{-1}$, $H_2 = 124.6\text{kJ} \cdot \text{kg}^{-1}$, $H_3 = 0$, and $H_4 = -88\text{kJ} \cdot \text{kg}^{-1}$. The kinetic parameters for the fourth reaction are: $K_{04} = 1.1 \times 10^5 \text{s}^{-1}$ and $E_4 = 100\text{kJ} \cdot \text{mol}^{-1}$. The kinetic parameters of reactions (1), (2), and (3) remain the same as the parameters presented in Table 1.

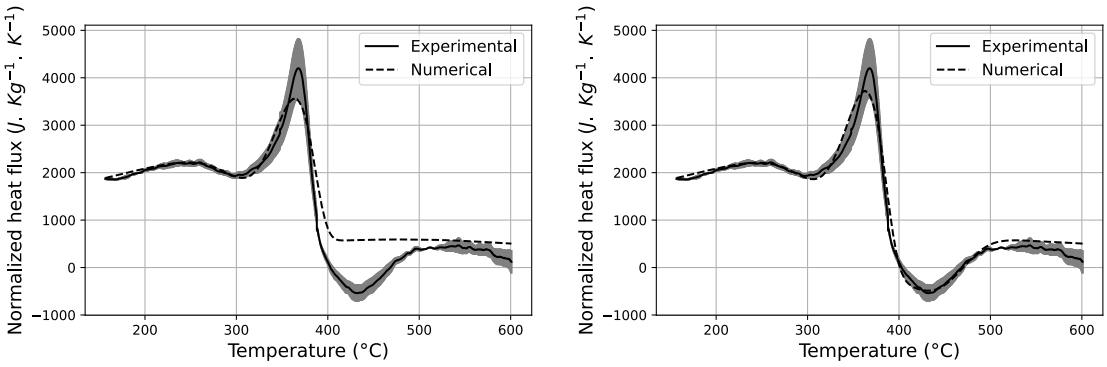


(a) 3 reactions (b) 4 reactions

Fig. 3. Comparison between the normalized heat flux measured by DSC and the numerical heat flux predicted with the model using (a) 3 reactions and (b) 4 reactions. The experimental data is the average of three repeatability tests.

## 3. Cone calorimeter scale

This section is dedicated to the study of spruce wood degradation under inert atmosphere at the cone calorimeter scale. At this scale, heat transfer cannot be neglected.

### 3.1 Materials and methods

The aim of this work was to model the thermal degradation of spruce wood in an inert atmosphere at the cone calorimeter scale, following the work of Terrei *et al.* [8]. These authors carried out cone calorimeter experiments with spruce wood samples (0.1 × 0.1 × 0.05 $\text{m}^3$) oriented vertically. During the tests, the samples were placed in a stainless-steel chamber. Continuous argon injection at a low flow rate maintained an oxygen concentration less than 3 % inside the chamber to prevent char oxidation. The sides and rear of the chamber were cooled down by water heat exchangers. The heat flux coming from the cone passes through a sapphire window placed on the front face of the chamber. Wood samples were placed in a calcium silicate sample holder (3 cm thick) to reduce lateral convection losses. The mass loss of the samples was measured by a weighing scale with 0.01 g accuracy. Twelve K-type 0.1 mm diameter thermocouples were embedded in the samples at different depths (2, 4, 6, 8, 10, 12, 14, 16, 18, 20, 30 and 40 mm), along the centerline of the samples, following the technique developed in Terrei *et al.*'s study [24]. Tests were performed at 35 and 45 $\text{kW} \cdot \text{m}^{-2}$. Further details about the experimental protocol can be found in [8].

Since several physical and chemical phenomena occur during wood experiments, it is difficult to characterize the thermal boundary conditions for the sample inside a chamber, in particular considering that the sapphire window is heated up during the experiment. Therefore, tests with an inert material were performed inside the chamber under the same

conditions as the wood tests *i.e.* same heat fluxes, argon flow rate and sample holder. In this case, only heat transfer occurs and it is easier to characterize the boundary conditions such as convection and radiative heat losses. The chosen inert material was low density calcium silicate (Silcal 1100®) since its thermal properties are close to those of spruce wood: the specific heat is around 1000 $\mathrm{J \cdot kg^{-1} \cdot K^{-1}}$ and the thermal conductivity varies between 0.08 and 0.2 $\mathrm{W \cdot m^{-1} \cdot K^{-1}}$ depending on the temperature [25]. Twelve thermocouples were also embedded along the centerline of the calcium silicate sample at the same depths as the wood samples. Moreover, an additional thermocouple was fixed at the rear face of the sample.

### 3.2 3D heat transfer model and estimation of the boundary conditions

A 3D heat transfer model was developed in PYTHON environment. The heat transfer balance described by eq. 12 was numerically solved using a finite volume method. For temporal discretization, an explicit scheme was used.

$$\rho C_p(T)\frac{\partial T}{\partial t} = \nabla \cdot \left(\bar{\bar{\lambda}}_c(T)\nabla T\right) \tag{12}$$

$\bar{\bar{\lambda}}_c$ is the thermal conductivity tensor. For calcium silicate, it reduces to a scalar because it is isotropic, but this will not be the case for wood. The boundary conditions are given in Fig. 4. Where: $h_{\mathrm{front}}$ and $h_{\mathrm{lateral}}$ are the convective heat transfer coefficients for

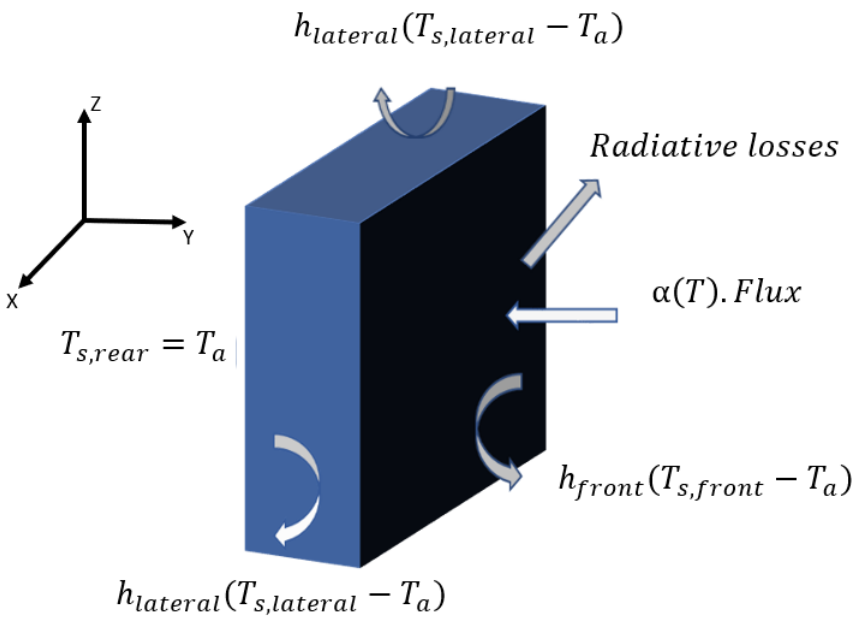


Fig. 4. Boundary conditions of a sample exposed to the cone calorimeter.

respectively the front and the lateral faces. $T_{\mathrm{S,front}}$, $T_{\mathrm{S,rear}}$ and $T_{\mathrm{S,lateral}}$ are the surface temperature for respectively the front, the rear and the four lateral faces. $\alpha(T)$ is the absorptivity. $T_a$ is the temperature of the atmosphere inside the steel chamber, assumed to be equal to the temperature measured at the back of the sample. Radiative losses depend on the radiative heat flux exchanged between the front of the sample and the sapphire window. Sapphire is a non grey and semi transparent material. Its spectral reflectivity $R(\lambda)$ ($\lambda$ being the wavelength) and transmissivity ($\mathrm{Tr}(\lambda)$) were measured using

a Fourier Transform Infrared (FTIR) Spectrometer. Calcium silicate is considered to be a non grey and opaque material. Its spectral reflectivity was also measured using FTIR spectroscopy. Absorptivity and emissivity were obtained from the radiative energy balance *i.e.* $\alpha(\lambda) = 1 - \mathrm{Tr}(\lambda) - R(\lambda)$ and Kirchhoff law ($\epsilon(\lambda) = \alpha(\lambda)$). The sample radiative losses are thus modelled as

$$\phi = \pi \int \left[ \frac{\epsilon_1(\lambda)\epsilon_2(\lambda)}{\epsilon_1(\lambda) + \epsilon_2(\lambda) - \epsilon_1(\lambda)\epsilon_2(\lambda)} \left( I_\lambda^{bb}(T_1) - I_\lambda^{bb}(T_2) \right) - \mathrm{Tr}_1(\lambda)\epsilon_2(\lambda) I_\lambda^{bb}(T_2) \right] \mathrm{d}\lambda \quad (13)$$

subscript 1 refers to the sapphire and subscript 2 to the sample (here the calcium silicate). $I_\lambda^{bb}(T)$ is the blackbody intensity (Planck function). The first term corresponds to the radiative heat exchange between the sapphire surface and the sample (if sapphire is hotter than the sample, this term is positive and corresponds to an energy gain, otherwise it is negative and it is an energy loss). The second term corresponds to the radiative heat flux emitted by the sample and transmitted through the sapphire window. The integral has been approximated by the rectangular method with a $\Delta\lambda = 0.2$ $\mu$m interval.
The temperature of the sapphire window was measured as a function of the exposure time (the sapphire window is heated up during the experiment) by an infrared camera (FLIR SC7300 LW) equipped with a 7.9 $\mu$m optical bandpass filter. At this wavelength sapphire is opaque and almost black (0.98 emissivity). The radiation emitted by the cone and reflected by the sapphire surface was subtracted from the measured radiation to only measure the radiation emitted by the sapphire window, following the procedure described in [26].
The heat capacity of the calcium silicate was measured as a function of temperature in [25] and was found to be equal to: $C_p(T) = 439 + 83\log_{10}(T + 273)$ where T is the temperature in °C. The density of calcium silicate was measured and found to be 240 $\mathrm{kg \cdot m^{-3}}$. The thermal conductivity ($\lambda_c$) was assumed to vary with the temperature according to a second degree polynomial:

$$\lambda_c(T) = \lambda_{c1}T^2 + \lambda_{c2}T + \lambda_3 \quad (14)$$

Where $\lambda_{c1}$, $\lambda_{c2}$ and $\lambda_{c3}$ are three constants to be estimated. An inverse method was applied on the temperature measurements obtained from the inert atmosphere calcium silicate tests at 35 and 45 $\mathrm{kW \cdot m^{-2}}$ using this model to characterize the boundary conditions. The objective function described by eq. 15 was minimized using the Levenberg-Marquardt algorithm.

$$S = \sum_{i=1}^{N} \left[ T_{exp}(t_i) - T_{mod}(t_i) \right]^2 \quad (15)$$

Where: N is the number of experimental points, $T_{exp}(t_i)$ and $T_{mod}(t_i)$ are respectively the measured temperature and the temperature calculated by the 3D heat transfer model. The minimization was performed using the two heat fluxes simultaneously to estimate $h_{front}$ and the thermal conductivity of the calcium silicate. Although the thermal conductivity of the calcium silicate was measured as function of temperature in Jannot *et al.*'s study [25], this property was kept as unknown in order to check the reliability of the parameters obtained by optimisation. Thus, an estimated thermal conductivity by inverse method close to the thermal conductivity measured experimentally by the hot wire technique [25] indicates that the convective heat transfer coefficient obtained by optimisation is reliable. $h_{\mathrm{lateral}}$ was supposed to be equal to 10 $\mathrm{W \cdot m^{-2} \cdot K^{-1}}$. In fact, a sensitivity analysis showed

that the measured temperatures are not sensitive to $h_{\text{lateral}}$, which makes sens because of the insulating role of the calcium silicate sample holder. It is therefore not possible to estimate this parameter by inverse method.

### 3.3 3D pyrolysis model and thermo-physical properties of wood

The 3D heat transfer model was coupled with the kinetic model in order to predict the thermal degradation of spruce wood in an inert atmosphere at the cone calorimeter scale. The following assumptions were made for the 3D pyrolysis model:

- Heat and mass transfer in the gas phase were not considered in the model.
- Effect of shrinking, cracking and swelling were neglected.

The degradation of wood occurs following the kinetic scheme presented in the matter scale section. The heat capacity of spruce wood was measured between 30 and 100 °C in 10 °C increments using a DSC SETARAM microdSc3 instrument. The heat capacity obtained is $C_{p,wood}(T) = 1131 + 4.67T$ where T is in °C. The latter correlation was extrapolated for the higher temperatures. The heat capacity of char was also measured between 30 and 600 °C and the heat capacity obtained is $C_{p,char}(T) = 693 + 3.44T$. The effective heat capacity was calculated as in equation 8. More details on the measurement technique of the heat capacity will be published in a future paper. Therefore, the energy conservation equation is as follow:

$$\frac{\partial}{\partial t}\left(\rho.C_p.T\right) = \nabla \cdot \left(\bar{\bar{\lambda}}_c(T)\nabla T\right) + k_1.\rho_1.H_1 + k_2.\rho_2.H_2 + k_3.\rho_3.H_3 + k_4.\rho_{C_2}.H_4 \qquad (16)$$

Where: $\rho$ is the bulk density calculated by $\rho = \rho_1 + \rho_2 + \rho_3 + \rho_{C_2} + \rho_{C_3} + \rho_{C_4}$; $\rho_1$, $\rho_2$, $\rho_3$, $\rho_{C_2}$, $\rho_{C_3}$ and $\rho_{C_4}$ are the mass of respectively the constituents $A_1$, $A_2$, $A_3$, $C_2$, $C_3$ and $C_4$ per unit volume. The thermal boundary conditions are given in Fig. 4 and the convective heat transfer coefficients are those estimated from the calcium silicate tests. The emissivity of the sample surface was measured as a function of the exposure time to the cone heater [8]. In the present model, the mean of the latter measurements was used *i.e.* 0.9 and the absorptivity was considered equal to the emissivity, since wood is almost grey and the surface chars quite rapidly, and char is even greyer than wood. The thermal conductivity of spruce wood was measured between 30 and 160 °C in the two directions parallel and perpendicular to the fiber direction [27] using the anisotropic parallel hot wire technique [28]. The latter measurements show that the transverse thermal conductivity increase from 0.096 $\text{W}\cdot\text{m}^{-1}\cdot\text{K}^{-1}$ at 20 °C to 0.110 $\text{W}\cdot\text{m}^{-1}\cdot\text{K}^{-1}$ at 160 °C. Meanwhile, the longitudinal thermal conductivity was found to be almost independent of temperature and equal to 0.345 $\text{W}\cdot\text{m}^{-1}\cdot\text{K}^{-1}$. It is worth noting that several studies have shown that the radial and tangential thermal conductivity of wood are similar [29, 30, 31, 32, 33]. Therefore, the thermal conductivities used in the model below the onset of pyrolysis were $\lambda_{c\perp} = 0.102$ $\text{W}\cdot\text{m}^{-1}\cdot\text{K}^{-1}$ in the transverse direction (radial and tangential) and $\lambda_{c\parallel} = 0.345$ $\text{W}\cdot\text{m}^{-1}\cdot\text{K}^{-1}$ in the longitudinal direction. Above 200 °C, the model assumes that the longitudinal thermal conductivity remains constant and the transverse thermal conductivity depends only on temperature according to the following law:

$$\lambda_{c\perp} = 0.102 + \lambda_1.(T - 200) + \lambda_2.(T - 200)^2 \qquad (17)$$

Where T is the temperature in °C, $\lambda_1$ and $\lambda_2$ were chosen in order to give a calculated mass loss, a calculated mass loss rate and calculated in-depth temperatures similar to

those obtained from the cone calorimeter tests on spruce under inert atmosphere. The thermal conductivity tensor is therefore

$$\bar{\bar{\lambda}}_c = \begin{pmatrix} \lambda_{c\perp} & 0 & 0 \\ 0 & \lambda_{c\perp} & 0 \\ 0 & 0 & \lambda_{c\parallel} \end{pmatrix} \tag{18}$$

$x$-axis is horizontal parallel to the exposed surface, $y$-axis is parallel to the cone heat flux and $z$-axis is vertical (thus wood fibers are oriented vertically), as shown in Fig. 4. Finally, a perfect thermal contact was considered between the wood sample and the calcium silicate sample holder and the thermal properties of the latter material were taken from the work of Jannot *et al.* [25].

## 4. Results and discussion

### 4.1 Calcium silicate tests for estimation of boundary conditions

Fig. 5 shows the experimental in-depth temperatures at 35 and 45 kW · m$^{-2}$ and their comparison with the numerical temperatures.

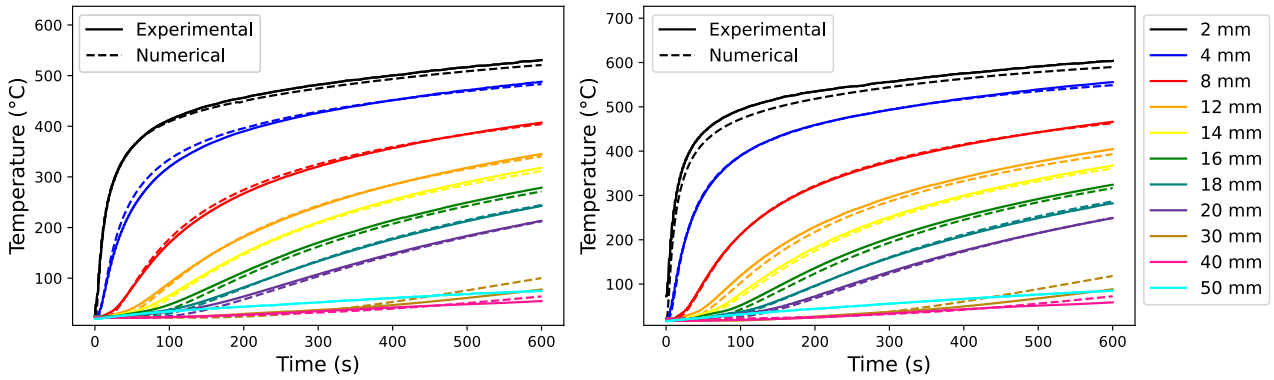


(a) 35 kW · m$^{-2}$ (b) 45 kW · m$^{-2}$

Fig. 5. Comparison between numerical and experimental in-depth temperature within the calcium silicate sample at two different heat fluxes.

The temperature measured at the rear face of the sample (50 mm) is higher than the temperature at 40 mm depth at the beginning of the test, indicating that the atmosphere inside the chamber is heated during the tests. The numerical and the experimental temperatures are in good agreement. The root-mean-square error obtained simultaneously for the two tests is 7 °C and the normalized root-mean-square error (NRMSE) is approximately 1.2 %. Fig. 6 shows the comparison between the estimated thermal conductivity and the thermal conductivity measured by the hot wire technique [25]. The two conductivies look very similar, almost linear with temperature, same slope, there is only a slight shift between them. The mean deviation between the estimated and the measured thermal conductivity is approximately 11.6 %. This is satisfactory considering i) the temperature measurement uncertainties (thermocouple accuracy and thermocouple position uncertainty), ii) that the inherent uncertainty of the hot wire technique used to measure the thermal conductivity is about 10 % [25] and iii) that the heat flux applied to the front of the sample was assumed to be homogeneous (which is not exactly the case[1]). This is

[1] consideration of a non-uniform heat flux will be investigated in the near future

very reassuring for the reliability of the results. The convective heat transfer coefficient obtained is $h_{front} = 31\ \mathrm{W \cdot m^{-2} \cdot K^{-1}}$.

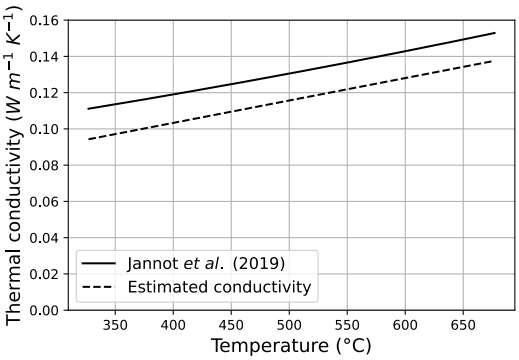


Fig. 6. Comparison between the estimated and the measured thermal conductivity of the calcium silicate [25].

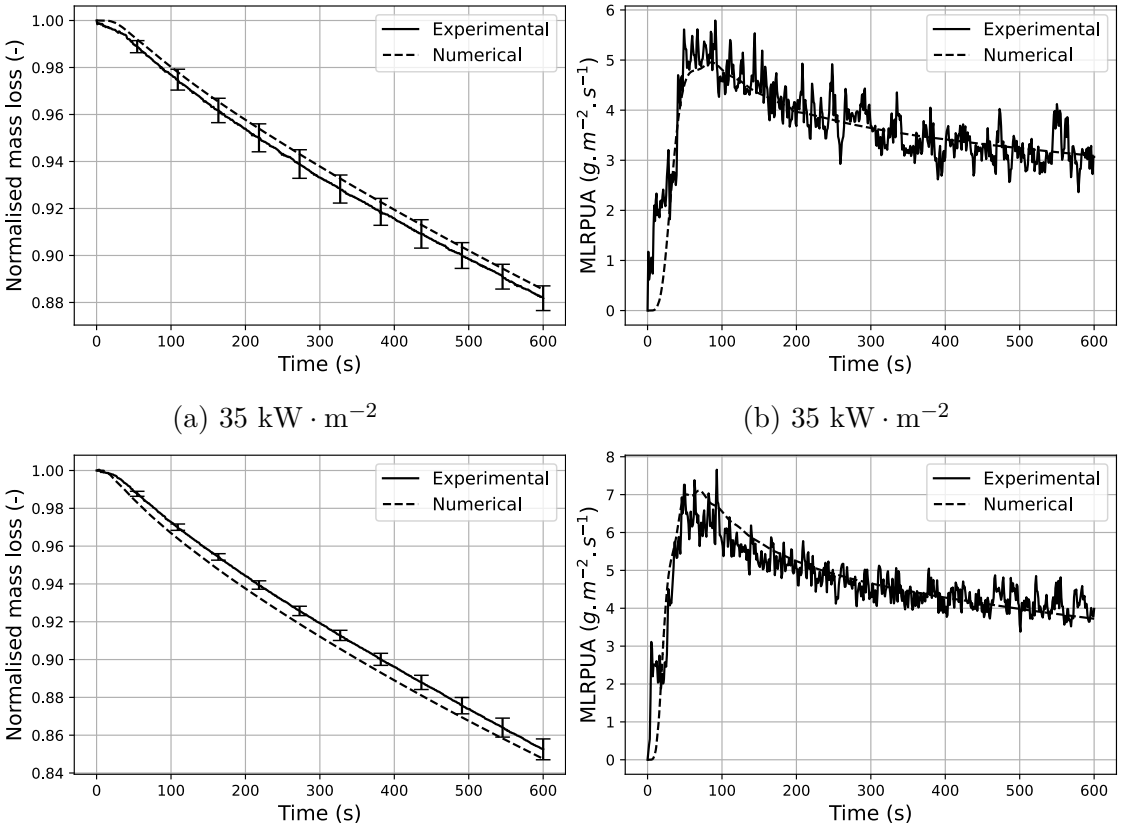


(a) $35\ \mathrm{kW \cdot m^{-2}}$ (b) $35\ \mathrm{kW \cdot m^{-2}}$

(c) $45\ \mathrm{kW \cdot m^{-2}}$ (d) $45\ \mathrm{kW \cdot m^{-2}}$

Fig. 7. Comparison between numerical and experimental mass loss and MLRPUA for wood tests at different heat fluxes.

## 4.2 Wood degradation at the cone calorimeter scale

As shown in the section 4.1, all properties of wood and calcium silicate were measured except thermal conductivity of wood/char above 200 °C. In addition, the boundary conditions were estimated from experiments with an inert material. Probably the convective

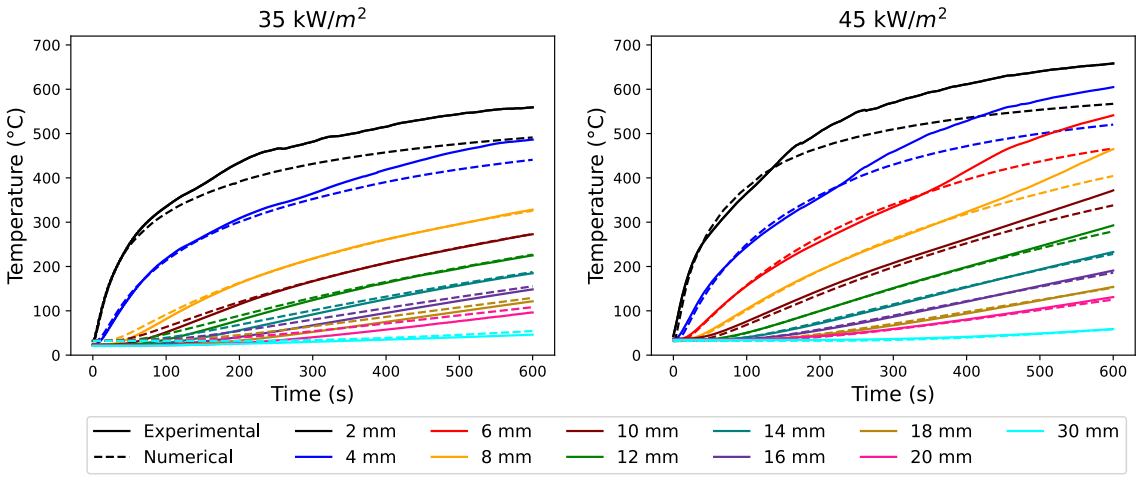


Fig. 8. Comparison between numerical and experimental in-depth temperature within the wood samples at different heat fluxes.

heat transfer coefficient could vary between calcium silicate and wood experiments, especially for the face exposed to the cone calorimeter. However, at least the order of magnitude of the convection losses was obtained. Several simulations were carried out by varying the thermal conductivity of wood above 200 °C. The thermal conductivity that gave the better agreement with the experimental mass loss and the mass loss per unit area (MLRPUA) is as follows:

$$\lambda_{c\perp} = 0.102 + 8.1 \times 10^{-7}.(T - 200)^2 \tag{19}$$

Where T is in °C. Fig. 7 shows the comparison between experimental and numerical MLRPUA at heat fluxes 35 and 45 $kW \cdot m^{-2}$. Concerning mass loss, the normalized root mean squared error (NRMSE) obtained between numerical and experimental results is respectively 3.2 and 4.2 %. Meanwhile, the NRMSE obtained between numerical and experimental MLRPUA is 6 and 5.6 % at respectively 35 and 45 $kW \cdot m^{-2}$. All these results show the robustness of the numerical model to evaluate the mass loss and the MLRPUA at different heat fluxes.

Fig. 8 shows the comparison between numerical and experimental in-depth temperatures for the two heat fluxes. Below 400 °C, numerical and experimental temperatures comply very well. However, above 400 °C the pyrolysis model underestimates the temperature. It is interesting to note that the TGA analysis showed that spruce wood loses more than 75 % of its initial weight between 200 and 400 °C *i.e* more than 89 % of the degradation was already occured below this temperature. Therefore, although there is a bias between experimental and numerical in-depth temperature at high temperatures, the model predicts the mass loss and MLRPUA well at the different heating fluxes. The discrepancy between numerical and experimental temperatures at high temperatures could be caused by several reasons. Firstly, at high temperatures the wood turns to char, its porosity becomes very high and consequently the thermocouple is no longer in good contact with the material. The second reason is that the model considers a homogeneous medium, whereas when wood chars, cracks appear and the model no longer applies. Finally, the main reason is that although the atmosphere was inerted, smoldering combustion, *i.e.* char oxidation, can occur at a low rate because the oxygen content was not exactly zero. However, temperature and MLR predictions obtained with the model proposed in this paper have been significantly improved compared to our previous work [8].

## 5. Conclusion

In this work, a 3D heat transfer and pyrolysis model for spruce wood was developed at the cone calorimeter scale under inert atmosphere. First, the thermal degradation of spruce wood was studied by TGA under inert atmosphere between ambient temperature and 1000 °C at different heating rates (5, 10 and 20 $K \cdot min^{-1}$). A global three-reaction mechanism was used to predict the mass loss and the mass loss rate. The kinetic parameters were estimated by fitting TGA data. The numerical and experimental results were in good agreement at this scale, where the wood sample is thermally thin and temperature gradients are negligible. Moreover, DSC measurements were carried out under an inert atmosphere at a heating rate of 10 $K \cdot min^{-1}$. It was found that the kinetic scheme with three reactions is unable to predict the heat flux measured by DSC. A fourth reaction was therefore added. Based on the DSC and ATG measurements, as well as previous measurements of the heat capacity of wood and char, the heat of pyrolysis of spruce wood was modeled as a function of temperature. At a larger scale, cone calorimeter tests were then carried out with an inert material in an inert atmosphere at 35 and 45 $kW \cdot m^{-2}$. The aim was to characterize the heat transfer boundary conditions for tests performed on wood samples under the same conditions. An inverse method was applied to the in-depth temperatures within a low density calcium silicate sample using a 3D heat transfer model to estimate the convective heat coefficients and thermal conductivity of that sample. The results showed that the thermal conductivity of calcium silicate obtained by optimization was in good agreement with the thermal conductivity measured by the hot wire technique. Therefore, the other parameters obtained from optimization, such as the convective heat transfer coefficient, can be considered reliable. Finally, a 3D pyrolysis model was developed by coupling the kinetic model, whose parameters were obtained from TGA, with a 3D heat transfer model. The boundary conditions estimated from the calcium silicate tests were fixed. All properties of wood were measured experimentally such as emissivity, absorptivity, heat capacity of wood until 100 °C, heat capacity of char until 600 °C, thermal conductivity in transverse and longitudinal direction until 160 °C. The heats of reaction were also determined using the DSC technique. The only property that remained unknown was the thermal conductivity above 200 °C. This latter property was varied until a good fit was obtained between the numerical mass loss, mass loss rate and in-depth temperatures and their experimental counterparts. The results obtained with the 3D pyrolysis model developed and presented in this work comply very satisfactorily with the experimental results and the thermal conductivity obtained above 200 °C sounds physical.

## Acknowledgements

LCPP (Laboratoire Commun de la Prefecture de Police) and LRGP (Laboratoire Réactions et Génie des Procédés) are fully acknowledged for TGA measurements and DSC measurements respectively.

## References

[1] R. Sikkema, D. Styles, R. Jonsson, B. Tobin, and K.A. Byrne. “A market inventory of construction wood for residential building in Europe – in the light of the Green Deal and new circular economy ambitions”. In: *Sustainable Cities and Society* 90

(2023), p. 104370. ISSN: 2210-6707. DOI: https://doi.org/10.1016/j.scs.2022.104370.

[2] Jakob Hildebrandt, Nina Hagemann, and Daniela Thrän. "The contribution of wood-based construction materials for leveraging a low carbon building sector in europe". In: *Sustainable Cities and Society* 34 (2017), pp. 405–418. ISSN: 2210-6707. DOI: https://doi.org/10.1016/j.scs.2017.06.013.

[3] Lei Wang, Anne Toppinen, and Heikki Juslin. "Use of wood in green building: a study of expert perspectives from the UK". In: *Journal of Cleaner Production* 65 (2014), pp. 350–361. ISSN: 0959-6526. DOI: https://doi.org/10.1016/j.jclepro.2013.08.023.

[4] C. A. Koufopanos, A. Lucchesi, and G. Maschio. "Kinetic modelling of the pyrolysis of biomass and biomass components". en. In: *Can. J. Chem. Eng.* 67.1 (Feb. 1989), pp. 75–84. ISSN: 00084034, 1939019X. DOI: 10.1002/cjce.5450670111.

[5] Carmen Branca and Colomba Di Blasi. "Kinetics of the isothermal degradation of wood in the temperature range 528–708 K". en. In: *J. Anal. Appl. Pyrolysis* (2003), p. 13.

[6] Zhihua Chen, Mian Hu, Xiaolei Zhu, Dabin Guo, Shiming Liu, Zhiquan Hu, Bo Xiao, Jingbo Wang, and Mahmood Laghari. "Characteristics and kinetic study on pyrolysis of five lignocellulosic biomass via thermogravimetric analysis". In: *Bioresource Technology* 192 (2015), pp. 441–450. ISSN: 0960-8524. DOI: https://doi.org/10.1016/j.biortech.2015.05.062.

[7] B. M. Wagenaar, Wolter Prins, and W.P.M. van Swaaij. "Pyrolysis of biomass in the rotating cone reactor: modelling and experimental justification". In: *Chemical Engineering Science* 49 (1994), pp. 5109–5126.

[8] Lucas Terrei, Guillaume Gerandi, Hassan Flity, Virginie Tihay-Felicelli, Zoubir Acem, Gilles Parent, and Paul-Antoine Santoni. "Experimental and numerical multi-scale study of spruce wood degradation under inert atmosphere". en. In: *Fire Safety Journal* 130 (June 2022), p. 103598. ISSN: 03797112. DOI: 10.1016/j.firesaf.2022.103598.

[9] H. Thunman, B. Leckner, F. Niklasson, and F. Johnsson. "Combustion of wood particles - a particle model for eulerian calculations". en. In: *Combustion and Flame* 129.1-2 (Apr. 2002), pp. 30–46. ISSN: 00102180. DOI: 10.1016/S0010-2180(01)00371-6.

[10] S. Benkorichi, T. Fateh, F. Richard, J.-L. Consalvi, and A. Nadjai. "Investigation of thermal degradation of pine needles using multi-step reaction mechanisms". en. In: *Fire Safety Journal* 91 (July 2017), pp. 811–819. ISSN: 03797112. DOI: 10.1016/j.firesaf.2017.03.058.

[11] Carmen Branca, Alessandro Albano, and Colomba Di Blasi. "Critical evaluation of global mechanisms of wood devolatilization". en. In: *Thermochimica Acta* 429.2 (May 2005), pp. 133–141. ISSN: 00406031. DOI: 10.1016/j.tca.2005.02.030.

[12] Morten Gunnar GrÃ¸nli, GÃ¡bor VÃ¡rhegyi, and Colomba Di Blasi. "Thermogravimetric Analysis and Devolatilization Kinetics of Wood". In: *Ind. Eng. Chem. Res.* 41.17 (Aug. 2002). Publisher: American Chemical Society, pp. 4201–4208. ISSN: 0888-5885. DOI: 10.1021/ie0201157.

[13] T. Kashiwagi, T.J. Ohlemiller, and K. Werner. “Effects of external radiant flux and ambient oxygen concentration on nonflaming gasification rates and evolved products of white pine”. en. In: *Combustion and Flame* 69.3 (Sept. 1987), pp. 331–345. ISSN: 00102180. DOI: 10.1016/0010-2180(87)90125-8.

[14] Chris Lautenberger and Carlos Fernandez-Pello. “Generalized pyrolysis model for combustible solids”. In: *Fire Safety Journal* 44.6 (2009), pp. 819–839. ISSN: 0379-7112. DOI: https://doi.org/10.1016/j.firesaf.2009.03.011.

[15] Stanislav I. Stoliarov, Sean Crowley, Richard N. Walters, and Richard E. Lyon. “Prediction of the burning rates of charring polymers”. In: *Combustion and Flame* 157.11 (2010), pp. 2024–2034. ISSN: 0010-2180. DOI: https://doi.org/10.1016/j.combustflame.2010.03.011.

[16] Lucas Bustamante Valencia. “Experimental and numerical investigation of the thermal decomposition of materials at three scales: application to polyether polyurethane foam used in upholstered furniture”. PhD thesis. ISAE-ENSMA Ecole Nationale Supérieure de Mécanique et d’Aérotechique-Poitiers, 2009.

[17] Franz Richter and Guillermo Rein. “A multiscale model of wood pyrolysis in fire to study the roles of chemistry and heat transfer at the mesoscale”. In: *Combustion and Flame* 216 (2020), pp. 316–325. ISSN: 0010-2180. DOI: https://doi.org/10.1016/j.combustflame.2020.02.029.

[18] Chris Lautenberger and Carlos Fernandez-Pello. “A model for the oxidative pyrolysis of wood”. In: *Combustion and Flame* 156.8 (2009), pp. 1503–1513. ISSN: 0010-2180. DOI: https://doi.org/10.1016/j.combustflame.2009.04.001.

[19] Haiping Yang, Rong Yan, Hanping Chen, Dong Ho Lee, and Chuguang Zheng. “Characteristics of hemicellulose, cellulose and lignin pyrolysis”. en. In: *Fuel* 86.12-13 (Aug. 2007), pp. 1781–1788. ISSN: 00162361. DOI: 10.1016/j.fuel.2006.12.013.

[20] Vaibhav Dhyani and Thallada Bhaskar. “A comprehensive review on the pyrolysis of lignocellulosic biomass”. en. In: *Renewable Energy* 129 (Dec. 2018), pp. 695–716. ISSN: 09601481. DOI: 10.1016/j.renene.2017.04.035.

[21] Donald W. Marquardt. “An Algorithm for Least-Squares Estimation of Nonlinear Parameters”. en. In: *Journal of the Society for Industrial and Applied Mathematics* 11.2 (June 1963), pp. 431–441. ISSN: 0368-4245, 2168-3484. DOI: 10.1137/0111030.

[22] Junhui Gong and Lizhong Yang. “A Review on Flaming Ignition of Solid Combustibles: Pyrolysis Kinetics, Experimental Methods and Modelling”. In: *Fire Technology* (2022), pp. 1–98.

[23] J. Rath, M.G. Wolfinger, G. Steiner, G. Krammer, F. Barontini, and V. Cozzani. “Heat of wood pyrolysis”. In: *Fuel* 82.1 (2003), pp. 81–91. ISSN: 0016-2361. DOI: https://doi.org/10.1016/S0016-2361(02)00138-2.

[24] Lucas Terrei, Zoubir Acem, Véronique Marchetti, Paul Lardet, Pascal Boulet, and Gilles Parent. “In-depth wood temperature measurement using embedded thin wire thermocouples in cone calorimeter tests”. en. In: *International Journal of Thermal Sciences* 162 (Apr. 2021), p. 106686. ISSN: 12900729. DOI: 10.1016/j.ijthermalsci.2020.106686.

[25] Yves Jannot and Alain Degiovanni. "An improved model for the parallel hot wire: Application to thermal conductivity measurement of low density insulating materials at high temperature". en. In: *International Journal of Thermal Sciences* 142 (Aug. 2019), pp. 379–391. ISSN: 12900729. DOI: 10.1016/j.ijthermalsci.2019.04.026.

[26] Zoubir Acem, Damien Brissinger, Anthony Collin, Gilles Parent, Pascal Boulet, Thi Hay Yen Quach, Benjamin Batiot, Franck Richard, and Thomas Rogaume. "Surface temperature of carbon composite samples during thermal degradation". In: *International Journal of Thermal Sciences* 112 (2017), pp. 427–438. ISSN: 1290-0729. DOI: https://doi.org/10.1016/j.ijthermalsci.2016.11.007.

[27] Hassan Flity, Yves Jannot, Lucas Terrei, Paul Lardet, Vincent Schick, Zoubir Acem, and Gilles Parent. "Thermal conductivity parallel and perpendicular to fibers direction and heat capacity measurements of eight wood species up to 160 °C". In: *International Journal of Thermal Sciences* submitted (2023).

[28] Yves Jannot, Alain Degiovanni, Vincent Schick, and Johann Meulemans. "Apparent thermal conductivity measurement of anisotropic insulating materials at high temperature by the parallel hot-wire method". en. In: *International Journal of Thermal Sciences* (2021), p. 9.

[29] S. Lagüela, P. Bison, F. Peron, and P. Romagnoni. "Thermal conductivity measurements on wood materials with transient plane source technique". en. In: *Thermochimica Acta* 600 (Jan. 2015), pp. 45–51. ISSN: 00406031. DOI: 10.1016/j.tca.2014.11.021.

[30] V. Hankalin, T. Ahonen, and R. Raiko. "On thermal properties of a pyrolysing wood particle". English. In: *Finnish-Swedish Flame Days 2009, January 28-29, 2009, Naantali, Finland*. 2009, 16 p.

[31] S. Korkut, A. Aytin, Ç. Tasdemir, and L. Gurau. *The transverse thermal conductivity coefficients of wild cherry wood heat-treated using the thermowood method*. Pro Ligno, Brasov, Romania, pp. 679-683. Nov. 2015.

[32] Hamiyet Kol. "The Transverse Thermal Conductivity Coefficients of Some Hardwood Species Grown in Turkey". en. In: *Forest Products Journal* 59.10 (Oct. 2009), pp. 58–63. ISSN: 0015-7473. DOI: 10.13073/0015-7473-59.10.58.

[33] Anna Dupleix, Andrzej Kusiak, Mark Hughes, and Fréderic Rossi. "Measuring the thermal properties of green wood by the transient plane source (TPS) technique". en. In: *Holzforschung* 67.4 (May 2013), pp. 437–445. ISSN: 1437-434X, 0018-3830. DOI: 10.1515/hf-2012-0125.

## Figure captions